Ground-state wave function of plutonium in PuSb as determined via x-ray magnetic circular dichroism

M. Janoschek, D. Haskel, J. Fernandez-Rodriguez, M. van Veenendaal, J. Rebizant, G. H. Lander, J.-X. Zhu, J. D. Thompson, and E. D. Bauer

The Ground State Wavefunction of Plutonium in PuSb as determined via X-ray Magnetic Circular Dichroism

M. Janoschek,[1, *] D. Haskel,[2] J. Fernandez-Rodriguez,[2, 3] M. van Veenendaal,[2, 3]
J. Rebizant,[4] G. H. Lander,[4] J.-X. Zhu,[1] J. D. Thompson,[1] and E. D. Bauer[1]

[1]*Los Alamos National Laboratory, Los Alamos, New Mexico 87545, USA*
[2]*Advanced Photon Source, Argonne National Laboratory, Argonne, Illinois 60439, USA*
[3]*Department of Physics, Northern Illinois University, DeKalb, Illinois 60115, USA*
[4]*European Commission, JRC, Institute for Transuranium Elements, 76125 Karlsruhe, Germany*
(Dated: December 19, 2014)

Measurements of x-ray magnetic circular dichroism (XMCD) and x-ray absorption near-edge structure (XANES) spectroscopy at the Pu $M_{4,5}$ edges of the ferromagnet PuSb are reported. Using bulk magnetization measurements and a sum rule analysis of the XMCD spectra, we determine the individual orbital ($\mu_{\mathrm{L}} = 2.8(1)\mu_{\mathrm{B}}$/Pu) and spin moments ($\mu_{\mathrm{S}} = -2.0(1)\mu_{\mathrm{B}}$/Pu) of the Pu $5f$ electrons for the first time. Atomic multiplet calculations of the XMCD and XANES spectra reproduce well the experimental data and are consistent with the experimental value of the spin moment. These measurements of $\langle L_z \rangle$ and $\langle S_z \rangle$ are in excellent agreement with the values that have been extracted from neutron magnetic form factor measurements, and confirm the local character of the $5f$ electrons in PuSb. Finally, we demonstrate that a split M_5 as well as a narrow M_4 XMCD signal may serve as a signature of $5f$ electron localization in actinide compounds.

PACS numbers: 75.25.-j,78.70.Dm, 71.20.Lp, 71.27.+a

I. INTRODUCTION

An understanding of the electronic structure throughout the actinide series remains an important but unsolved problem in condensed matter physics. This lack of understanding is most apparent in plutonium, which is at the boundary of an itinerant to localized crossover of the $5f$ electrons that is reflected in Pu's six allotropic phases with large changes in volume between them of up to 25%.[1] Conventional electronic structure calculations do not capture this behavior, but instead predict a volume of the cubic δ-Pu phase some 30% smaller than is observed, leading to a predicted magnetically ordered ground state that experiments demonstrate is not correct.[2] Instead, plutonium is an intermediate-valence ground state involving charge fluctuations between three $5f^4$, $5f^5$, and $5f^6$ electronic configurations,[3] producing an electronic structure that is arguably the most complex of all the elements. Dynamical Mean Field Theory calculations show promise for accounting for some of the unusual behavior of Pu's $5f$ electrons, including the intermediate valence ground state,[4] but the starting point for a complete understanding of the electronic structure of the actinides must come from experiments and theoretical calculations on Pu materials situated at the simpler, localized or itinerant extremes of $5f$ electron behavior.

Here we investigate the behavior of PuSb that is in the localized $5f$ electron limit. PuSb crystallizes in the simple cubic NaCl structure with a lattice parameter a = 6.225 Å and shows two magnetic transitions, an antiferromagnetic transition at $T_N = 85$ K, followed by a ferromagnetic transition at $T_C = 67$ K. In the ferromagnetic state, magnetization measurements reveal a ordered magnetic moment $\mu_{\mathrm{ord}} = 0.67\mu_{\mathrm{B}}$/Pu along the easy [100] cubic axis, and a large magnetic anisotropy, indicating the influence of crystal fields.[5] Polarized neutron diffraction measurements have been employed to study the magnetic form factor of the $5f$ electrons

in PuSb.[6] Fits to the measured magnetic form factor show that it is described by a localized model using an intermediate coupling scheme assuming a $5f^5$ configuration and a Γ_8 crystal field ground state. These fits also provide evidence for the presence of anisotropic interactions, as highlighted by the extracted large orbital moment of $\mu_{\mathrm{L}} = 2.75\mu_{\mathrm{B}}$/Pu. The local character of the $5f$ electrons in PuSb is further underlined by inelastic neutron scattering experiments that show the presence of spin-wave like features typical of localized magnetic moments,[7] and by photoemission experiments that demonstrate the occupied $5f$ states are withdrawn to just below the Fermi level.[8] Thus, the body of available experimental data suggests that PuSb exists in the limit of localized $5f$ electrons. Indeed, DMFT calculations show that PuSb is a nearly integral-valent ($n_f = 5.0$), local-moment semi-metal.[9] Moreover, in calculations of the magnetic form factor, the large orbital moment is reproduced correctly[7,10]. However, no direct measurements of the orbital moment $\langle L_z \rangle$, spin moment $\langle S_z \rangle$, as well as the strength of spin-orbit coupling $\langle \mathbf{L} \cdot \mathbf{S} \rangle$, required for a full description of the electronic ground state of the $5f$ electrons in PuSb, have been performed. In this work, we report x-ray absorption near edge structure (XANES) and magnetic circular dichroism (XMCD) measurements to determine $\langle L_z \rangle$, $\langle S_z \rangle$, and $\langle \mathbf{L} \cdot \mathbf{S} \rangle$ in the ground state of PuSb via sum rules analysis.[11,12] Here we use the conventional description of $\mu_L = -\langle L_z \rangle$ and $\mu_S = -2\langle S_z \rangle$.[13]

II. EXPERIMENTAL DETAILS

Single crystals of PuSb were prepared by the recrystallization technique as described in Ref.14 approximately 20 years ago. Measurements at the M_4 (3.970 keV) and M_5 (3.775 keV) absorption edges of Pu were carried out on a PuSb single crystal in a fluorescence geometry using a 4-element silicon drift dioade fluorescence detector at beam line
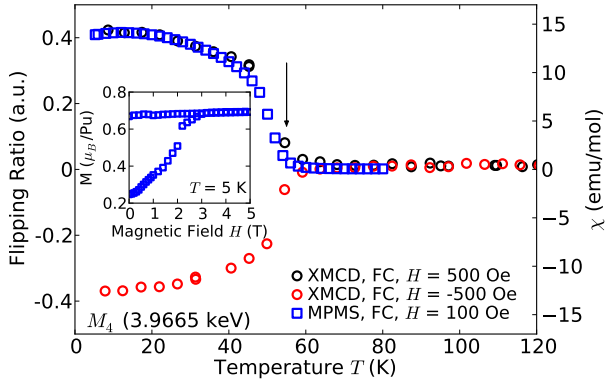
FIG. 1. Temperature dependence of the ferromagnetic signal in PuSb as obtained by XMCD and field-cooled (FC) magnetic susceptibility measurements. Black and red circles denote the flipping ratio as measured on the M_4-edge at 3.9665 keV for the magnetic field of $H = 500$ Oe directed parallel and antiparallel to the photon wave vector. The flipping ratio is defined as $\frac{\mu^+ - \mu^-}{\mu^+ + \mu^-}$, where μ^+ and μ^- denote data sets recorded with left- and right-circularly polarized x-rays, respectively. The blue squares denote magnetic susceptibility measurements carried out in $H = 100$ Oe. The black arrow marks the reduced ferromagnetic critical temperature T_C of the PuSb sample. The inset shows magnetization data obtained at a temperature $T = 5$ K from which a saturation moment $\mu_{sat} = 0.68$ μ_B/Pu was extracted.

4-ID-D of the Advanced Photon Source, Argonne National Laboratory. To prevent the spread of radioactive contamination, the sample was triply-contained in a custom-made holder. The sample holder was mounted on thermally conducting sapphire films in contact with a Cu holder that couples to the cold finger of a closed-cycle cryostat. A vacuum tight, doubled-wall, hat made of Cu and Kapton ceiling was bolted over the sample space and sealed with Indium wire for encapsulation. The helicity of a circularly polarized x-ray beam, generated with a 50 μm-thick diamond phase retarder,[15] was modulated at 13.55 Hz and the related modulation in the absorption coefficient measured with a phase lock-in amplifier.[16] The magnetic field was aligned parallel to a cubic axis of the sample and the photon wave vector. Each measurement was carried out after field-cooling in magnetic fields of $H = 500$ Oe directed along and opposite to the photon wave vector, respectively, to check for experimental artifacts.

Fig. 1 shows the flipping ratio measured at the M_4-edge of PuSb defined as $\frac{\mu^+ - \mu^-}{\mu^+ + \mu^-}$ as function of temperature T obtained on warming after field-cooling with a magnetic field $H = \pm 500$ Oe. Here μ^+ and μ^- denote fluorescence signals recorded with left- and right-circularly polarized x-rays, respectively. The flipping ratio is non-zero below $T_C = 55$ K due to the onset of ferromagnetic order. We note that the significant reduction of T_C of about 12 K is due to self-radiation damage of Pu-239 in the 20-year-old sample stored at room temperature. This was further confirmed by additional magnetic susceptibility measurements carried out in a Quantum Design Magnetic Property Measurement System during field-cooling in $H = 100$ Oe (see Fig. 1). The magnetization measurement confirm the drop in T_C, but the saturation moment
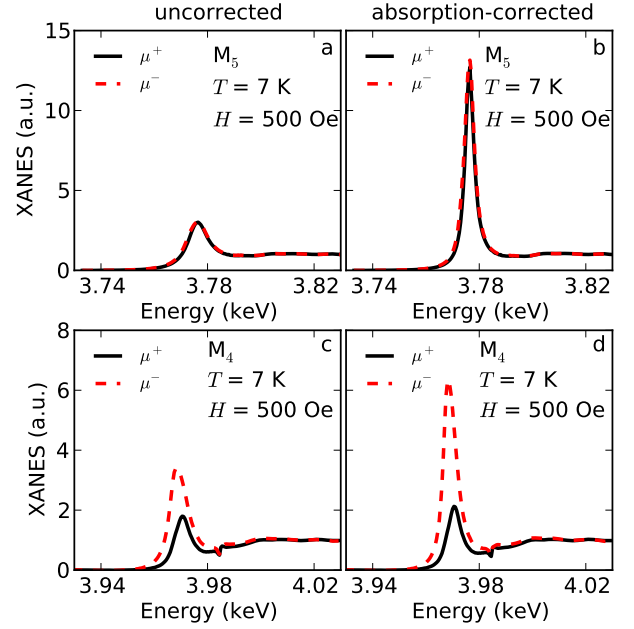

FIG. 2. The results of the self-absorption correction of our XANES data for PuSb are shown. For all data sets the edge-jump has been normalized to one. μ^+ and μ^- denote data sets recorded with left- and right-circularly polarized x-rays, respectively. (a) and (b) show scans performed over the M_5-edge of Pu, where in (a) the uncorrected and normalized raw-data are shown, whereas (b) illustrates the result of the self-absorption correction (see text for details). Similarly, scans shown in (c) and (d) were carried out around the M_4-edge where (c) is the uncorrected raw-data, and (d) gives the result of the correction.

deduced is 0.68 μ_B/Pu, in excellent agreement with the previous value of 0.67 μ_B/Pu.[5]

III. DATA ANALYSIS

The self-absorption correction carried out on the helicity-dependent flourescence XANES data is illustrated in Fig. 2. Self-absorption corrections measured with the the fluorescence technique are most significant when a heavy atom such as Pu is embedded in a host of lighter atoms. The correction can be performed using the following equation[17,18]

$$I_{cor}(\omega) = \frac{N\left(\frac{\mu_{tf}(\omega_f)}{\mu_e(\omega_0^+)} \frac{\sin \theta_i}{\sin \theta_f} + \frac{\mu_b(\omega_0^+)}{\mu_e(\omega_0^+)}\right)}{\left(\frac{\mu_{tf}(\omega_f)}{\mu_e(\omega_0^+)} \frac{\sin \theta_i}{\sin \theta_f} + \frac{\mu_b(\omega_0^+)}{\mu_e(\omega_0^+)} + 1\right) - N}, \quad (1)$$

where N is the background subtracted and edge-step normalized (edge is normalized to one) raw fluorescence data and I_{cor} is the self-absorption corrected data. Further, $\mu_{tf}(\omega_f)$ is the weighted total absorption cross-section (in barn/atom) of all atoms in the sample at the relevant fluorescence energy (here M_α/M_β of Pu), $\mu_e(\omega_0^+)$ is the absorption cross-section of the central atom (here Pu) above the resonant edge (M_5/M_4), and $\mu_b(\omega_0^+)$ is the absorption cross-section of all atoms below the resonant edge. The cross-sections used in this

TABLE I. Photon and absorption cross-sections for Pu and Sb at the photon energies of the M_5 (3775 eV) and M_4 (3970 eV) edges, as well as the fluorescence energies M_α (3339 eV) and M_β (3534 eV) of Pu that have been used to perform the self-absoprtion correction (cf. Eq. 1) of the fluorescence data sets on PuSb presented in this paper.

cross-section	M_5		M_4		M_α	M_β
(10^5 barn/atom)	below	above	below	above		
Pu	1.936	4.641	4.047	5.709	2.740	2.403
Sb	0.770		0.680		1.046	0.906
$\mu_{tf}(\omega_f)$	–		–		3.786	3.309
$\mu_e(\omega_0^+)$	2.704		1.661		–	–
$\mu_b(\omega_0^+)$	2.706		5.708		–	–

work have been taken from the XCOM Photon Cross Sections Database published by the National Institute of Standards and Technology and are listed in table I. θ_i and θ_f are the angles between the sample surface and the incident and final photon wave vectors, respectively. In our experiment they were $\theta_i = 90°$ and $\theta_f = 30°$. Figs. 2 (a) and (b) compare the raw and corrected fluorescence data for both helicities μ^+ and μ^- at the M_5-edge. It is immediately clear that the corrections are sizable as expected for a heavy central atom such as Pu, and highlight that the self-absorption correction is crucial to obtain correct results when performing XMCD measurements on Pu compounds. Figs. 2 (c) and (d) illustrate the effect of the correction at the M_4-edge. The implications of this correction on the size of extracted spin and orbital components of the magnetic moments will be discussed at the end of this section.

In Fig. 3 we show the normalized XANES ($\mu_0 = \frac{\mu^+ + \mu^-}{2}$) and XMCD ($\Delta\mu = \mu^+ - \mu^-$) data for PuSb that was obtained using the self-absorption corrected fluorescence data sets with left (μ^+) and right-handed (μ^-) helicity for both the M_5 and M_4-edges. We note that for correct normalization the edge-steps at the M_5 and M_4 edges have been normalized to one and 0.61 according to the edge-step-ratio $\mu_e(M_4)/\mu_e(M_5) = 0.61$ given in the XCOM cross sections. Whereas the orbital moment is obtained directly from XMCD, only an effective spin polarization $\mu_{s,eff}$, not the spin moment, may be determined. Using the sum rules for the M_5- and M_4-edges we extract the $5f$ orbital contribution to magnetic moment via

$$-\mu_L = \langle L_z \rangle = n_h \frac{\Delta I_{M_5} + \Delta I_{M_4}}{I_{M_5} + I_{M_4}}. \quad (2)$$

The effective spin polarization is given by

$$\langle S_{eff} \rangle = \langle S_z \rangle + 3\langle T_z \rangle = \frac{n_h}{2} \frac{\Delta I_{M_5} - \frac{3}{2}\Delta I_{M_4}}{I_{M_5} + I_{M_4}}, \quad (3)$$

with

$$-\mu_{s,eff} = 2\langle S_{eff} \rangle = 2\langle S_z \rangle + 6\langle T_z \rangle. \quad (4)$$

Here $\mu_s = -2\langle S_z \rangle$ is the spin moment, and $\mu_{md} = -6\langle T_z \rangle$ is the magnetic dipole contribution. The spin moment μ_s may be
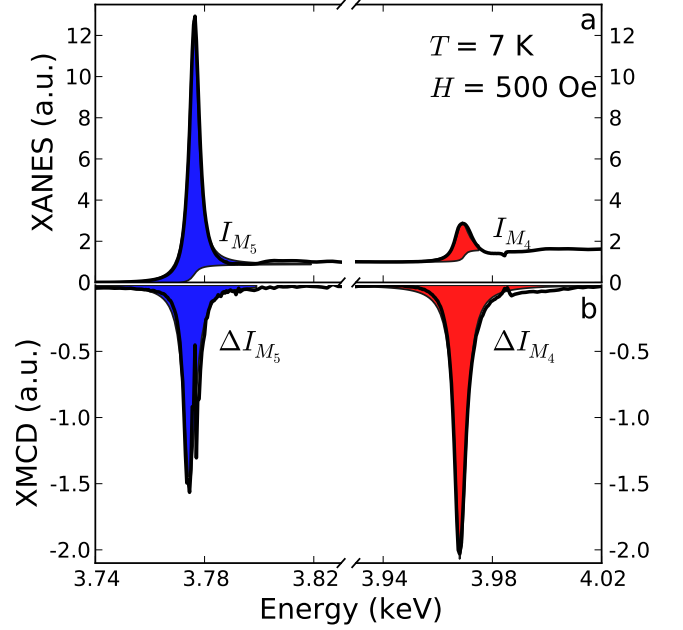

FIG. 3. Panels (a) and (b) show the XANES ($\frac{\mu^+ + \mu^-}{2}$) and XMCD ($\mu^+ - \mu^-$) data for PuSb, respectively, obtained from the absorption corrected spectra illustrated in Fig. 2 for both the M_4- and M_5-edges. The edge-jump for the M_5-edge has been normalized to one, whereas the M_4 is normalized to 0.61 according to the edge-step ratio between the two edges. The blue shaded regions in (a) and (b) denote the integrated intensity of the M_5 whiteline (I_{M_5}) and XMCD (ΔI_{M_5}) signals, whereas the red shades denote the integrated intensities I_{M_4} and (ΔI_{M_4}) at the M_4-edge.

determined using the combination of neutron scattering measurements which give the total magnetic moment and XMCD or by theoretical calculations, as described below. Further, n_h is the number of holes in the $5f$ shell, where $n_h = 9$ for the $5f^5$ configuration of Pu in PuSb. I_{M_4}/I_{M_5} are the integrated intensity in isotropic white lines at the M_4/M_5 edges, and $\Delta I_{M_4}/\Delta I_{M_5}$ are the integrated intensities in the partial dichroic signal (see shaded areas in Fig. 3). In addition, the strength of the spin-orbit coupling may be extracted by means of the branching ratio $B = I_{M_5}/(I_{M_5} + I_{M_4})$ and

$$\frac{2\langle L \cdot S \rangle}{3n_h} = -\frac{5}{2}\left(B - \frac{3}{5}\right) + \Delta, \quad (5)$$

where Δ generally depends on the exact electronic configuration; however for a $5f^5$ configuration as in PuSb the quantity Δ is zero[19].

Using Eqs. 2-5, we find the values for μ_L, $\mu_{s,eff}$ and $\frac{2}{3}\langle L \cdot S \rangle$ presented in table II. Further, because the total $5f$ moment is $\mu = \mu_s + \mu_L$ we can use the total moment measured by neutron scattering $\mu = 0.75(1)$ $\mu_B/$Pu[6] to deduce[20] the spin moment $\mu_s = -2.0(1)$. This also allows us to estimate the ratio between the orbital and the total magnetic moments $C_2 = \frac{\mu_L}{\mu_L + \mu_s}$, and the magnetic dipole contribution $\mu_{md} = \mu_{s,eff} - \mu_s$. Table II also compares our obtained results with both neutron form factor measurements (b)[6], and DMFT calculations (e)[10,21] and shows that the agreement

TABLE II. Various quantities derived via the application of XMCD sum rules (see text for details) are compared to results from neutron form factor measurements and theory. The five columns denote results that have been obtained using (a) a combination of XMCD and neutron diffraction, (b) neutron form factor measurements published in Ref.[6], (c) an atomic multiplet single ion code that treat intermediate coupling exactly and includes the effect of crystal fields (this work), (d) LDA+U calculations (this work), and finally (e) DFT/LDA+DMFT published in Ref.10. For (a) the first block of quantities is solely derived from the sum rules, whereas the second block uses the total Pu magnetic moment measured by neutron measurements 6. The values for the angular and spin components (marked with an $*$) in (b) were estimated using a model based on the intermediate coupling scheme and an Γ_8 crystal field state.[22]

Quantity (unit)	(a) XMCD+ Neutron	(b) Neutron [6]	(c) Atomic	(d) LDA+U	(e) DMFT
			Theory		
μ_L (μ_B/Pu)	2.8(1)	2.75*	2.77	2.37	–
$\mu_{s,eff}$ (μ_B/Pu)	-1.2(1)	–	-1.52	–	–
B	0.848(8)	–	0.80		–
$\frac{2}{3}\langle \mathbf{L}\cdot\mathbf{S}\rangle$	-5.6(2)	–	-4.91	–	-5.3[21]
μ (μ_B/Pu)	0.75(1)[6]	0.75(1)	0.65	0.27	–
μ_s (μ_B/Pu)	-2.0(1)	-2.0*	-2.12	-2.10	–
C_2	3.7(2)	3.80(7)	4.26	8.68	3.92[10]
μ_{md} (μ_B/Pu)	0.8(2)	–	0.60	–	–
μ_{md}/μ_s	-0.4(1)	–	-0.28	–	–
$\langle T_z\rangle$ (μ_B/Pu)	-0.13(3)	–	-0.10	–	–

with both is indeed excellent. We also note that the value $B = 0.848(5)$ for the branching ratio determined here, corresponds to an expectation value of the spin-orbit coupling of $\langle \mathbf{L}\cdot\mathbf{S}\rangle = -8.6$. This is significantly closer to the value $\langle \mathbf{L}\cdot\mathbf{S}\rangle = -10$ expected within jj coupling than the -3 expected for a Hund's rule ground state. The value is in good agreement with using an intermediate coupling scheme of the spin and orbital moments,[19] as generally expected for actinides, and also consistent with the neutron form factor measurements.[6]

Finally, we discuss the effects of the employed self-absorption correction on the size of spin and orbital moments extracted via the analysis described above. Using the data sets that were not corrected for self-absorption effects (cf. Fig. 1) we obtain that μ_L=3.0(1) μ_B/Pu. As above, by using the total magnetic moment determined via neutron scattering, the corresponding spin moments is μ_s = -2.3(1) μ_B/Pu. We note that these values are still in relatively good agreement with the results determined via neutron diffraction or theory (cf. II). Further, based on the small difference with respect to the values determined from the corrected XMCD spectra, we estimate that the error bar associated with the self-absorption correction is less than 0.1 μ_B/Pu.

IV. THEORY AND COMPARISON WITH EXPERIMENT

We performed atomic multiplet calculations[23] of PuSb to compute the XANES and XMCD spectra. Here, the use of full configuration interaction allows for an exact treatment of
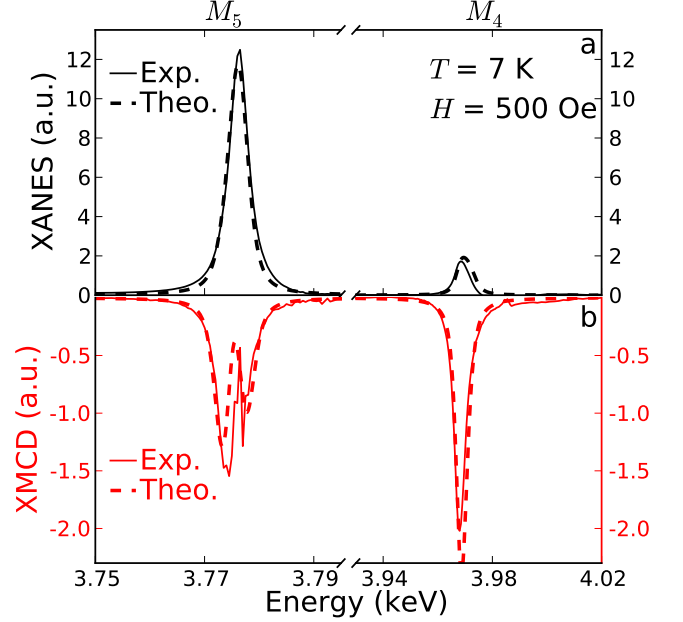

FIG. 4. Panels (a) compares the whiteline (black solid lines, obtained by removing the background and the edge-jump from the XANES data in Fig. 3(a))intensities to atomic multiplet single ion code simulations (black broken lines, see text for details) at the M_5- and M_4-edges, respectively. In (b) the measured XMCD signals (red solid lines) are compared to these simulations (red broken lines). We note that the XMCD signal at the M_5-edge is split into two peaks that are separated by approximately 3 eV. This is well captured by our atomic multiplet calculations and is discussed in detail in the text and Fig. 5.

intermediate coupling. We use Hartree-Fock estimates[24] of the spin-orbit coupling and Slater integrals (reduced at 80% of their atomic values) and a crystal field in O_h point symmetry to account for the partial magnetization of the Pu^{3+} ion. The results of the calculations are shown in Figs. 4(a) and (b) for the XANES and XMCD signal, respectively. The calculations are in excellent agreement with the experimental results.

We note that the splitting of the M_5 edge XMCD spectra is also well reproduced in the calculation. As we discuss below, the split M_5 XMCD peak is a signature of a strong Coulomb interaction and, hence, of localized $5f$ behavior, in agreement with the well-established localized character of the $5f$ electrons in PuSb.[5–10] From our atomic multiplet calculations that treats intermediate coupling exactly, we can study the effect of electron localization in PuSb by rescaling the Coulomb interactions in our multiplet calculations and see how this affects the x-ray absorption spectra. The reduction in the Coulomb parameters (Slater integrals) is related to an increase in metal-ligand hybridization and indicates a decrease in the importance of the Coulomb interaction. A strong reduction represents the situation where the excitonic final states probed by XAS are not completely pulled below the valence band continuum. In Fig. 5(a) we show the calculated XMCD signals for Slater integral reduction from $r = 0.8$ to 0.6. A reduction of the Coloumb interaction results in the "compression" of the atomic multiplet structure with a concomitant reduction in the
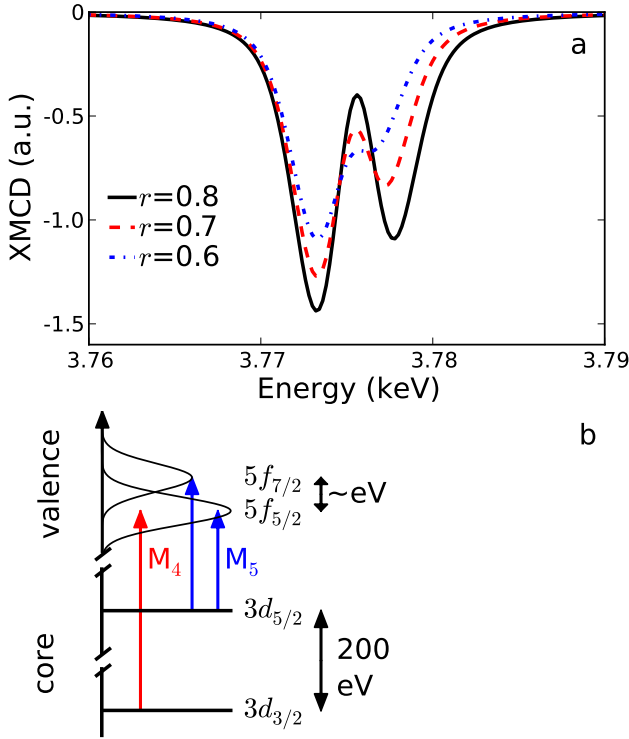
FIG. 5. (a) Results of our atomic multiplet calculations for the M_5 edge XMCD for different rescalings r of the Slater integrals that parametrize the Coulomb interaction. The structure of the M_5 XMCD spectrum is mainly due to Coulomb multiplet interactions. Strong hybridization with Sb would result in a compression of the spectral line shape which can be mimicked by a reduction of r. The absence of a strong reduction and the pronounced presence of the high-energy shoulder leads to the conclusion that the absorption edge is excitonic, which is indicative of localization of the $5f$ electrons. (b) Schematic illustrating the difference in intensity of the two spin-orbit split edges. In the ground state, the electrons have predominantly $5f_{5/2}$ character. The empty states therefore have a significantly larger $5f_{7/2}$ character. Since the angular momentum change for dipolar transitions is less than 1, the spectral weight of the M_4 edge is suppressed since $5f_{7/2}$ cannot be reached from the $3d_{5/2}$ core level. Both j can however be reached from the $3d_{5/2}$ state. This explains why the experimental branching ratio of 0.848 is substantially larger that the statistical branching ratio of 0.6 expected from the degeneracies of the core levels. Note that this sum-rule argument only depends on the nature of the ground state and not on the detailed spectral line shape of the $M_{4/5}$ edges.

splitting of the M_5 edge XMCD signal. Thus, the presence of a large splitting in the experimental M_5 XMCD spectrum is a signature of strong Coulomb interactions and hence, of localized behavior. Resonant scattering experiments also observed the split Pu M_5 resonance some years ago, consistent with the present study.[25]

Another interesting aspect concerns the narrow linewidth (full-width at half maximum, FWHM) observed at the M_4 edge in PuSb. The FWHM of 5 eV is only slightly larger than expected from the instrumental resolution function convoluted with the intrinsic core-hole lifetime of 4 eV. A review

of XMCD measurements on U- and Np-compounds in Ref. 20 shows that in all such experiments a larger linewidth of ≈10 eV has been observed. This is also the case of the PuFe$_2$ M_4 XMCD spectra, and this was reproduced by LSDA+U calculations.

To understand qualitatively the intensity difference between the two different spin-orbit split edges, we note that at the M_4 edge the spectrum consists of transitions from the $3d_{3/2}$ core level into the unoccupied $5f_{5/2}$ levels as illustrated in Fig. 5(b). As one progresses across the actinide series there is a steady filling of the $j = 5/2$ states[26] until it is nominally full at Am. This is not strictly correct in intermediate coupling, but a good approximation. In fact the branching ratio, B, can be related to the occupation number $n_{5/2}$ of the $j = 5/2$ states,[20] which is over 4 electrons in PuSb (and PuFe$_2$). This implies less than two electron states above the Fermi energy E_F. For uranium systems, of course, the number of unoccupied states is much greater.

The energy FWHM of the M_4 XMCD, assuming the core $3d$ states are confined to a narrow energy range, will reflect the energy distribution of the $j = 5/2$ unoccupied states. In the case of PuSb these are narrow, because there is no strong hybridization, whereas in the case of PuFe$_2$ there is hybridization with the Fe $3d$ states, so the XMCD spectrum for this material at M_4 is wide. In each case, theory has reproduced the M_4 spectrum, albeit using different theoretical approaches.

The values for the spin and orbital parts of the magnetic moments, as well as the spin-orbit coupling extracted from these calculations are also shown in table II column (c), and demonstrate that this model is in excellent agreement with our experimental determination. These XMCD results coupled with the atomic multiplet calculations, determine the spin and orbital moment in PuSb for the first time, and demonstrate that this material is in the localized limit. To give a more comprehensive comparison, we also carried out the electronic structure calculations based on the density functional theory in the generalized gradient approximation (GGA).[27] A full-potential linearized augmented plane wave method as implemented in the WIEN2k code[28] was used. The spin-orbit coupling was included in the second-order variational approximation. An averaged value of on-site Coulomb interaction $U = 2.23$ eV was used while, as in Ref. 29, a non-spin-polarized exchange-correlation functional was enforced. As shown in Table II (column (d)) the electronic structure calculations failed to reproduce the orbital moment, even with the inclusion of a Coulomb U parameter. This is perhaps not so surprising, since LDA generally works well for itinerant, band-like $5f$ materials and not ones with localized $5f$ electrons, such as PuSb.

The amount of information so far available on transuranium materials for $\langle T_z \rangle$, or more usefully $\mu_{md}/\mu_s = -6\langle T_z \rangle/\mu_s$ is, at the moment, very limited, so it is hard to draw conclusions. The experimental entry in Table II gives a value of 0.8/(−2.0) = −0.4(1). This is quite different from that found for PuFe$_2$, where the value is +0.23(5).[20] Interestingly, the atomic theory value[13] for intermediate coupling is −0.22, and we have calculated −0.28, so we see that the PuSb value is much closer to atomic theory than in the case of PuFe$_2$. This again is ex-

pected for the localized $5f$ electrons in PuSb.

V. CONCLUSIONS

In summary, x-ray magnetic circular dichroism and x-ray absorption spectroscopy measurements have been performed on the ferromagnet PuSb. From a sum rule analysis of the XMCD spectra and the value of the total moment, as determined by neutrons,[6] we derive the individual values for the spin and orbital moments for the first time. Atomic multiplet calculations of the XMCD and XANES spectra reproduce well the experimental data and are consistent with the experimental value of the spin moment. These measurements of $\langle L_z \rangle$ and $\langle S_z \rangle$ are in excellent agreement with the values that have been extracted from the magnetic form factor measurements, as well as with DMFT results, and confirm the local character of the $5f$ electrons in PuSb.

We have also shown that the shapes of the M-edge spectra are important clues as to the behavior of the $5f$ electrons. As found in PuSb and PuFe$_2$[20] the spectra are different from one another. These differences reflect the fact that the $5f$ states are localized in PuSb and itinerant in PuFe$_2$.

Finally, the combination of XMCD measurements and the-ory on actinide systems promises to provide a stringent test for those theories, and is one of the "benchmark" techniques that help us to unravel the complexity of $5f$–electron systems. The XMCD technique requires only microgram samples, so may be extended further into the actinide series, where only small samples are available.

* Corresponding Author: mjanoschek@lanl.gov

[1] J. L. Smith, and E. A. Kmetko,, J. Less-Common Met. **90**, 83 (1983).

[2] J. C. Lashley *et al.*, Phys. Rev. B **72**, 054416 (2005).

[3] C.H. Booth, Yu Jiang, D.L. Wang, J.N. Mitchell, P.H. Tobash, E.D. Bauer, M.A. Wall, P.G. Allen, D. Sokaras, D. Nordlund, T.-C. Weng, M.A. Torrez, and J.L. Sarrao, PNAS **10** 10205 (2012)

[4] J. H. Shim , K. Haule, G. Kotliar Nature **446**, 513–516 (2007).

[5] B. R. Cooper, P. Thayamballi, J. C. Spirlet, W. Müller, and O. Vogt, Phys. Rev. Lett. **51**, 2418 (1983).

[6] G. H. Lander et al., Phys. Rev. Lett. **53**, 2262 (1984).

[7] G.H. Lander, W.G. Stirling, J. Rossat-Mignod, J.C. Spirlet, J. Rebizant, and O. Vogt, Physica B **136**, 409 (1986).

[8] T. Durakiewicz *et al.*, Phys. Rev. B **70**, 205103 (2004).

[9] C.-H. Yee, G. Kotliar, and K. Haule, Phys. Rev. B **81**, 035105 (2010).

[10] M. E. Pezzoli *et al.*, Phys. Rev. Lett. **106**, 016403 (2011).

[11] B. T. Thole, P. Carra, F. Sette, and G. van der Laan, Phys. Rev. Lett. **68**, 1943 (1992); P. Carra, B. T. Thole, M. Altarelli, and X. Wang, Phys. Rev. Lett. **70**, 694 (1993); C. T. Chen, Y. U. Idzerda, H. J. Lin, N. V. Smith, G. Meigs, E. Chaban, G. H. Ho, E. Pellegrin, and F. Sette, Phys. Rev. Lett. **75**, 152 (1995).

[12] G. van der Laan and B. T. Thole, Phys. Rev. Lett. **60**, 1977 (1988).

[13] G. van der Laan and B. T. Thole, Phys. Rev. B **53**, 14458, 1996.

[14] O. Vogt and K. Mattenberger, in Handbook on the Physics and Chemistry of Rare Earths, eds K. A. Gschneidner and L. Eyring (North-Holland, Amsterdam), Vol. 17, p. 301 (1993)

[15] K. Hirano, K. Izumi, T. Ishikawa, S. Annaka, and S. Kikuta, Jpn. J. Appl. Phys. **30**, L407 (1991); J. C. Lang and G. Srajer, Rev. Sci. Instrum. **66**, 1540 (1995).

[16] M. Suzuki, N. Kawamura, M. Mizumaki, A. Urata, H. Maruyama, S. Goto, and T. Ishikawa, Jpn. J. Appl. Phys. **37**, L1488 (1998).

[17] T.M. Hayes and J.B. Boyce, Solid State Physics **37**, 173 (1983).

[18] D. Haskel, FLUO: Correcting XANES for self-absorption in fluorescence measurements, http://www.aps.anl.gov/ haskel/fluo.html (1999).

[19] G. van der Laan, K. T. Moore, J. G. Tobin, B. W. Chung, M. A. Wall, and A. J. Schwartz, Phys. Rev. Lett. **93**, 097401 (2004).

[20] F. Wilhelm, R. Eloirdi, J. Rusz, R. Springell, E. Colineau, J.-C. Griveau, P. M. Oppeneer, R. Caciuffo, A. Rogalev, and G. H. Lander, Phys. Rev. B **88** 024424 (2013).

[21] J. H. Shim, K. Haule and G. Kotliar Europhys. Lett. **85**, 17007 (2009).

[22] G. H. Lander, Phys. Sripta **44**, 33 (1991).

[23] J. Fernandez-Rodriguez, B. Toby, and M. van Veenendaal, arXiv:1406.7532

[24] R. Cowan, The Theory of Atomic Structure and Spectra (1981).

[25] P. S. Normile, W. G. Stirling, D. Mannix, G. H. Lander, F. Wastin, J. Rebizant, and S. Coburn, Phys. Rev. **66**, 0144406 (2002).

[26] K. T. Moore, and G. van der Laan, Rev. Mod. Phys. **81**, 235 (2009).

[27] J. P. Perdew, S. Burke, and M. Ernzerhof, Phys. Rev. Lett. **77**, 3865 (1996).

[28] P. Blaha, K. Schwarz, G. K. H. Madsen, D. Kvasnicka, and J. Luitz *WIEN2k: An Augmented Plane Wave + Local Orbitals Program for Calculating Crystal Properties* (K. Schwarz, Tech. Universität Wien, Austria, 2001).

[29] A. O. Shorikov, A. V. Lukoyanov, M. A. Korotin, and V. I. Anisimov, Phys. Rev. B **72**, 024458 (2005).